

Supplementary Information

Electro Fenton's Reaction Coupled Zn-Air Battery for In-Situ Pollutant Degradation

Neethu Christudas Dargily^{a†}, Giddaerappa Kuntoji^{a†}, Rahul Mahadeo Mendhe^{a†}, Akshay Haridas^a, Ravikumar Thimmappa^a, Surbhi Sharma^b, Musthafa Ottakam Thotiyl^{a}*

^aDepartment of Chemistry and Centre for Energy Science, Indian Institute of Science Education and Research (IISER)-Pune, Dr. Homi Bhabha Road, Pashan, Pune 411008, Maharashtra, India

^bCentre for New Energy Transition Research (CfNETR), Federation University Australia, Gippsland Campus, 1 Northways Road, Churchill 3842, Australia

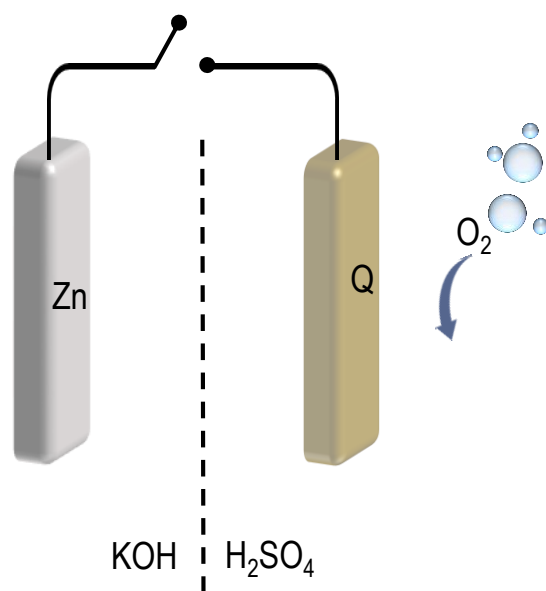
**Corresponding author*

† These authors contributed equally

Table of contents

Figures no	Descriptions	Page no
Schemes		
Scheme S1	Schematic representation of the battery architectural components.	4
Scheme S2	Reaction scheme for the electrochemical reduction of ethylanthraquinone and its chemical oxidation in presence of O ₂ to generate H ₂ O ₂ .	6
Scheme S3	Schematic representation showing the hydroxyl radical assisted degradation pathways of paracetamol.	11
Scheme S4	Schematic representation showing the hydroxyl radical assisted degradation pathways of phenol.	13
Calculation		
Calculation S1	Finding the number of electrons using Levich equation at various potentials.	8
Figures		
Figure S1	FTIR spectra of AQ and AQ/C composite materials.	4
Figure S2	FESEM images of the AQ/C composite at different magnification.	5
Figure S3	HRTEM images AQ/C composite at (a,b) different magnification.	6
Figure S4	Cyclic voltammograms of AQ/C electrode at different scan rates in 0.5 M H ₂ SO ₄ solution in (a) N ₂ saturated solution and (b) oxygen saturated solution.	7
Figure S5	Levich plot extracted from Figure 1e.	7
Figure S6	Calibration plot extracted from Figure 2d.	9

Figure S7	(a) XRD and (b) FTIR spectra of AQ/C composite electrode before and after battery discharge.	9
Figure S8	(a) pH of anodic and cathodic compartment under open circuit condition for a period of 24 hours. (b) OCV at t = 0 and t = 24 hr	10
Figure S9	Polarization curves of the Zn-air battery at varying conditions. (with and without Fe ²⁺ /Paracetamol / purging with N ₂ or O ₂ .)	10
Figure S10	(a) Time dependent UV-Vis spectra of the battery catholyte in absence of Fe ²⁺ ions. (b) NMR spectra of the catholyte before and after the battery discharge in absence of Fe ²⁺ ions.	11
Figure S11	(a) XRD and (b) FTIR spectra of AQ/C composite electrode before and after battery discharge.	12
Figure S12	The performance of the pollutant degrading air battery for multiple cycles in O ₂ purged H ₂ SO ₄ solution (pH 3) containing 0.2 mM Fe ²⁺ and paracetamol (0.5 mM). (a) Polarization curves of the Zn-air battery and (b) the corresponding galvanostatic polarization at 10 mA/cm ² .	12
Figure S13	(a) XRD and (b) FTIR spectra of AQ/C composite electrode before and after battery discharge.	13
Figure S14	UV-Vis spectra of the electrolyte before and after discharge at 5 mA/cm ² .	14
Figure S15	Degradation efficiency (%) demonstrated by various methods in comparison to this work.	14
References		15



Scheme S1. Schematic representation of the battery architectural components.

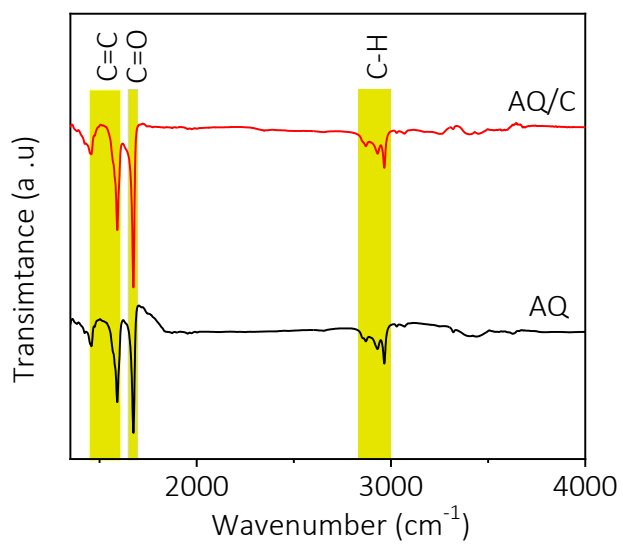


Figure S1. FTIR spectra of AQ and AQ/C composite materials.

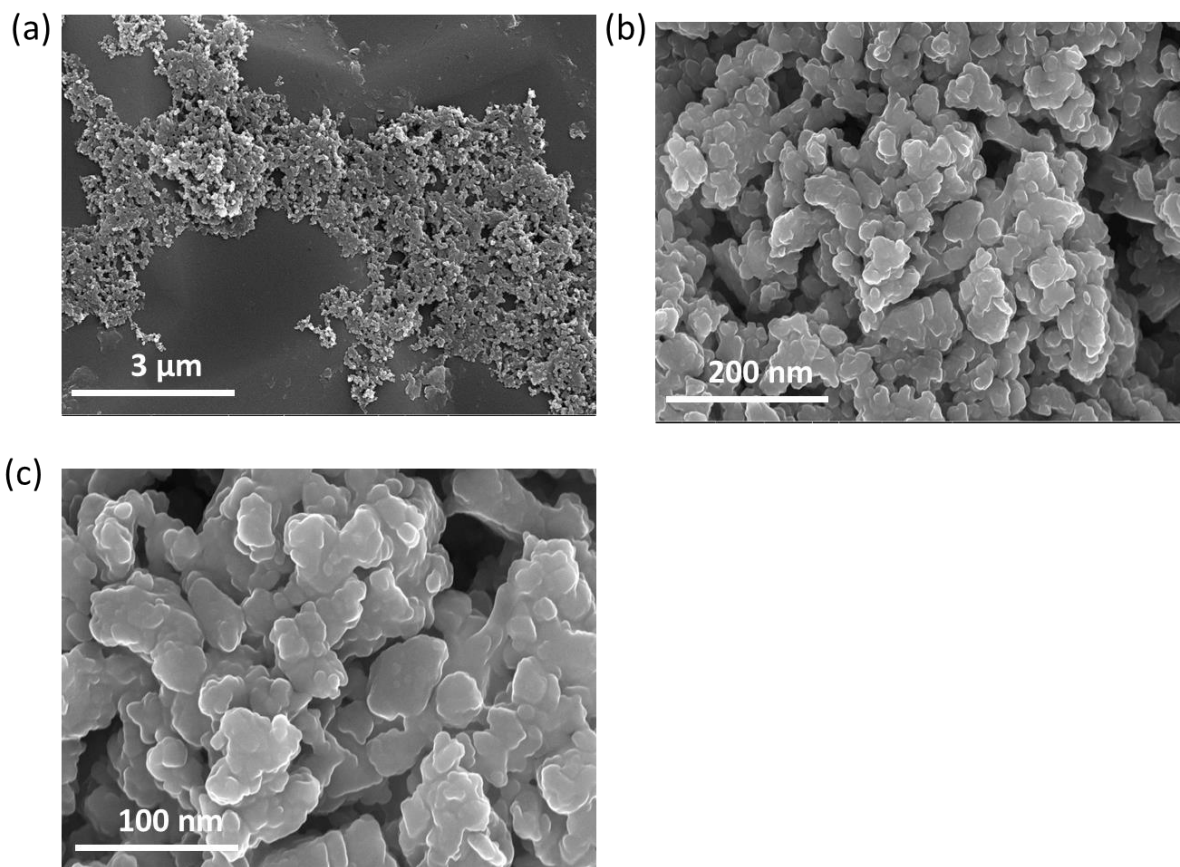


Figure S2. FESEM images of the AQ/C composite at different magnifications.

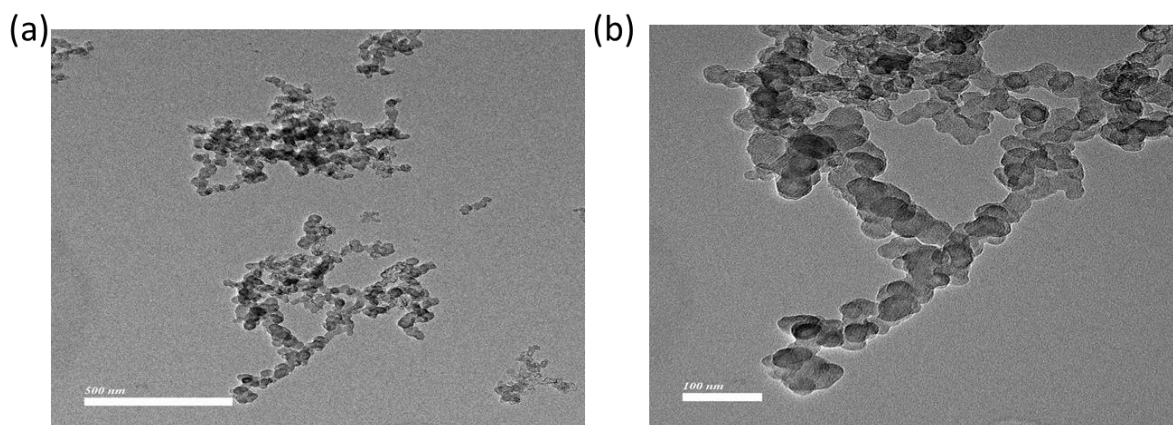
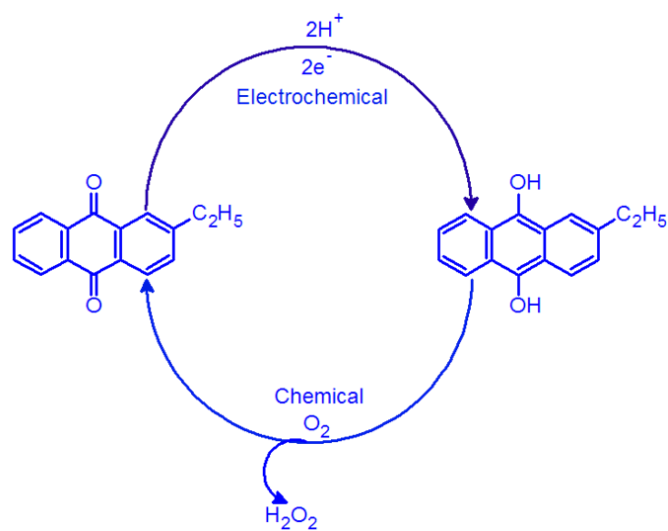


Figure S3. HRTEM images AQ/C composites at (a, b) different magnifications.



Scheme S2. Reaction scheme for the electrochemical reduction of ethylanthraquinone and its chemical oxidation in presence of O_2 to generate H_2O_2 . [Ref: 1, 2]

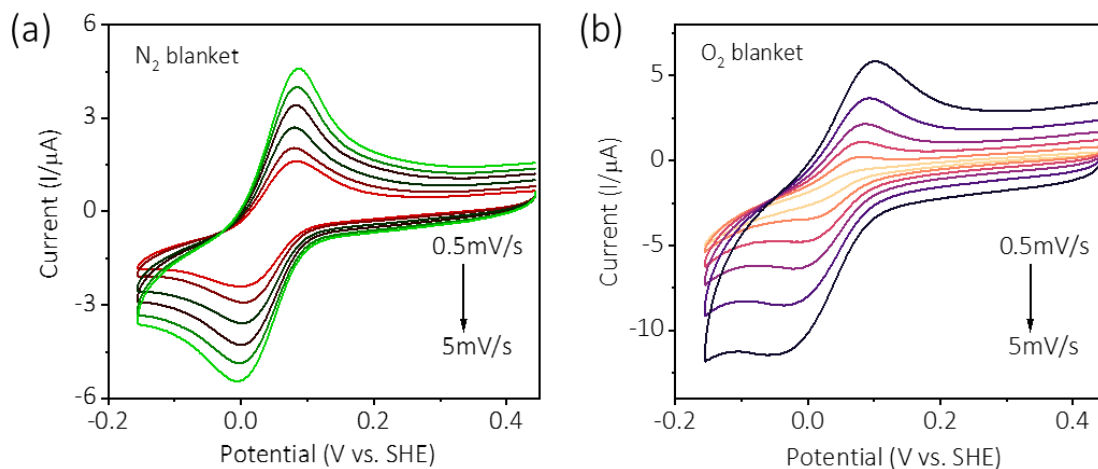


Figure S4. Cyclic voltammograms of AQ/C electrode at different scan rates in 0.5 M H₂SO₄ solution in (a) N₂saturated solution and (b) oxygen saturated solution.

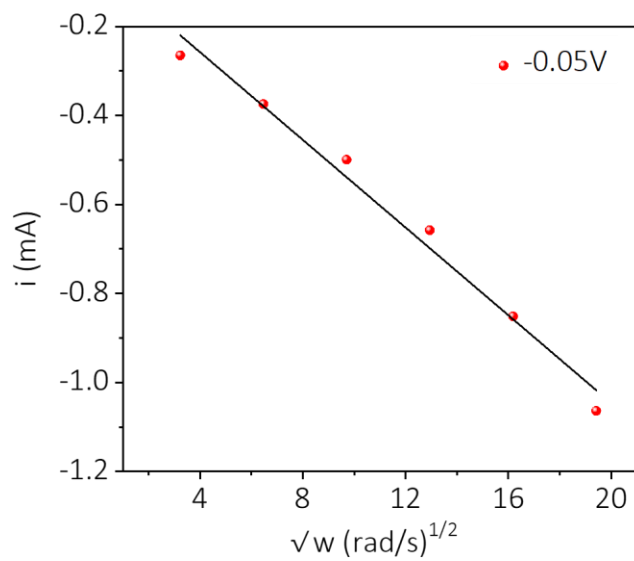


Figure S5. Levich plot extracted from Figure 1e.

Calculation S1.

Finding the number of electrons using Levich equation

$$1/\text{slope} = 0.62 n F A D^{(2/3)} u^{(-1/6)} C$$

where,

$$F = 96485.33 \text{ C/mol}$$

$$A = 0.196 \text{ cm}^2$$

$$D = 1.93 \times 10^{-5} \text{ cm}^2/\text{s}$$

$$\text{Kinematic viscosity } (u) = 0.0100$$

$$C = 1.26 \times 10^{-6} \text{ M/cm}^2$$

The Slope values were extracted from the Levich plot at 1600 RPM

$$\text{at } -0.05 \text{ V} = 4.9298 \text{ e}^{-5},$$

$$\text{at } -0.1 \text{ V} = 5.1148 \text{ e}^{-5},$$

$$\text{at } -0.15 \text{ V} = 5.5341 \text{ e}^{-5} \text{ and}$$

$$\text{at } -0.2 \text{ V} = 6.0313 \text{ e}^{-5}$$

Potential E(V) vs. SHE	No. of electrons from RRDE
-0.05 V	2.15
-0.1 V	2.23
-0.15 V	2.41
-0.2 V	2.63

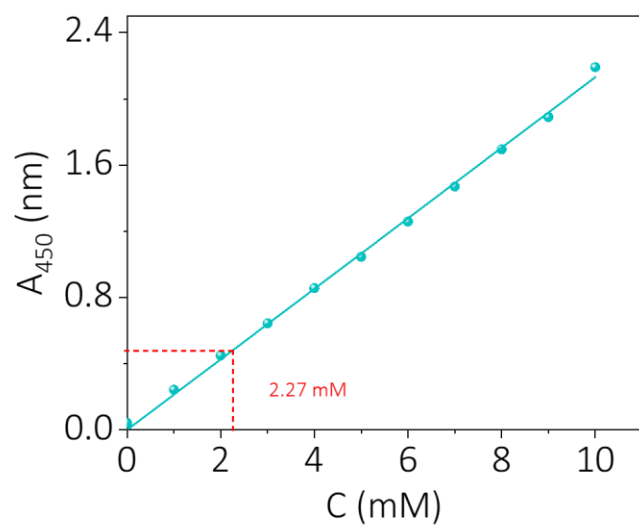


Figure S6. Calibration plot extracted from Figure 2d.

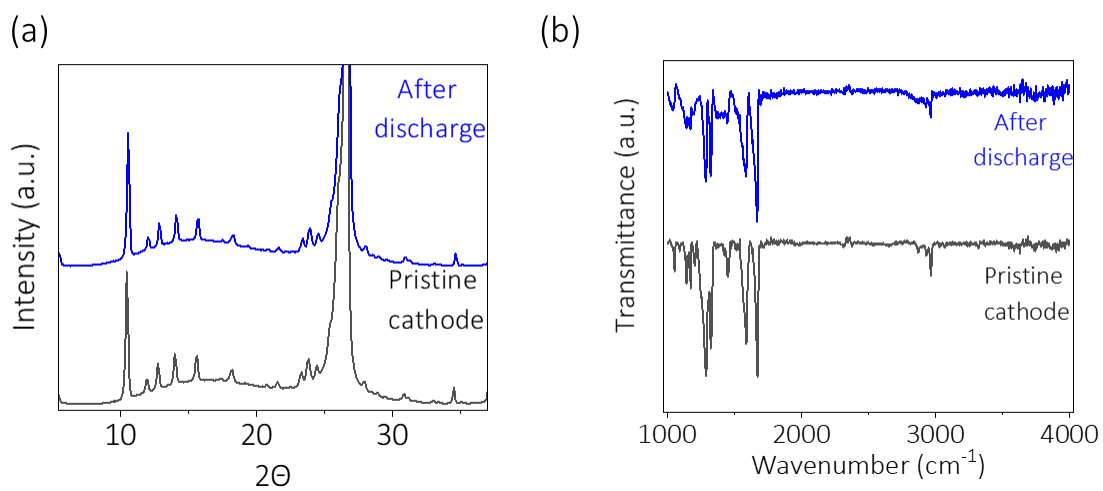


Figure S7. (a) XRD and (b) FTIR spectra of AQ/C composite electrode before and after battery discharge.

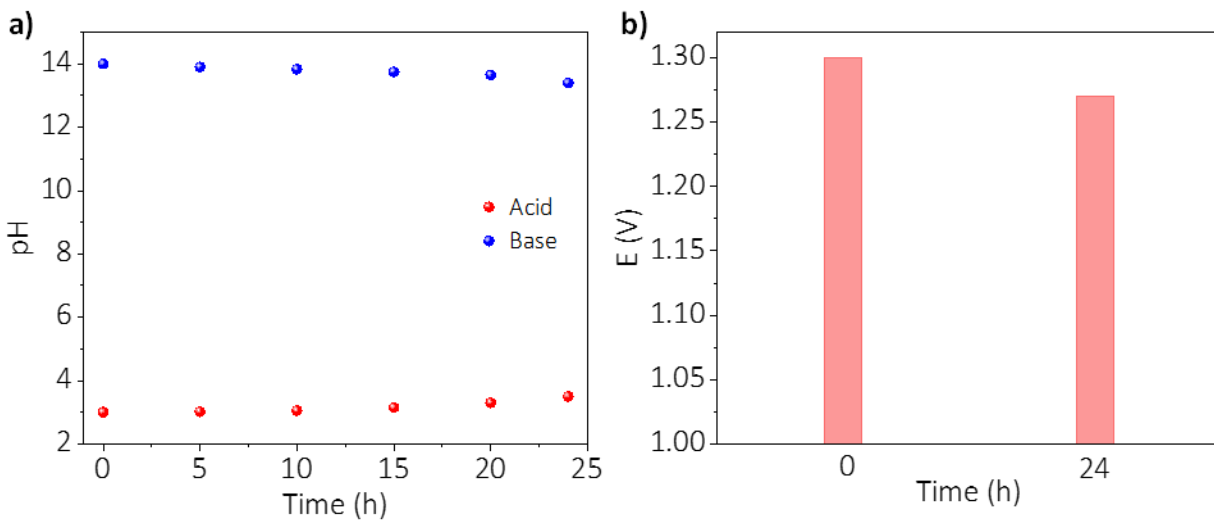


Figure S8. (a) pH of anodic and cathodic half-cells under open circuit condition (OCV) for a period of 24 hours. (b) OCV at t = 0 hr and t = 24 hr.

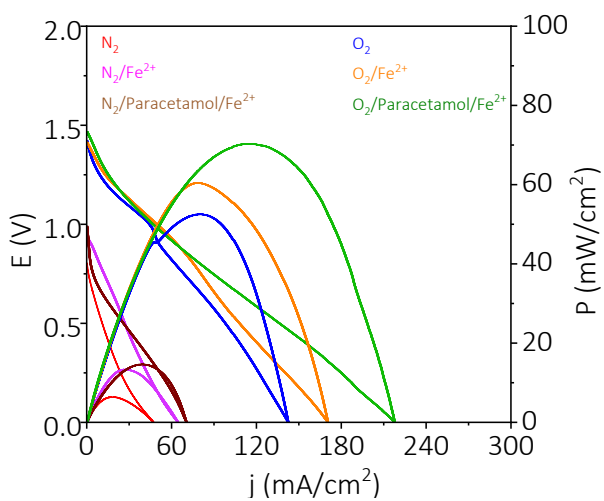


Figure S9. Polarization curves of the Zn-air battery at varying conditions (with and without Fe^{2+} /paracetamol / purging with N_2 or O_2).

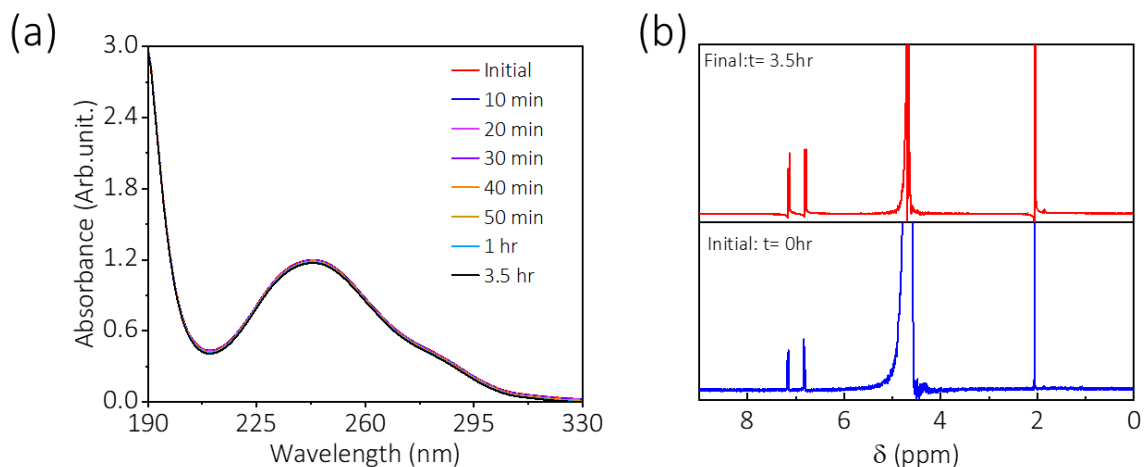
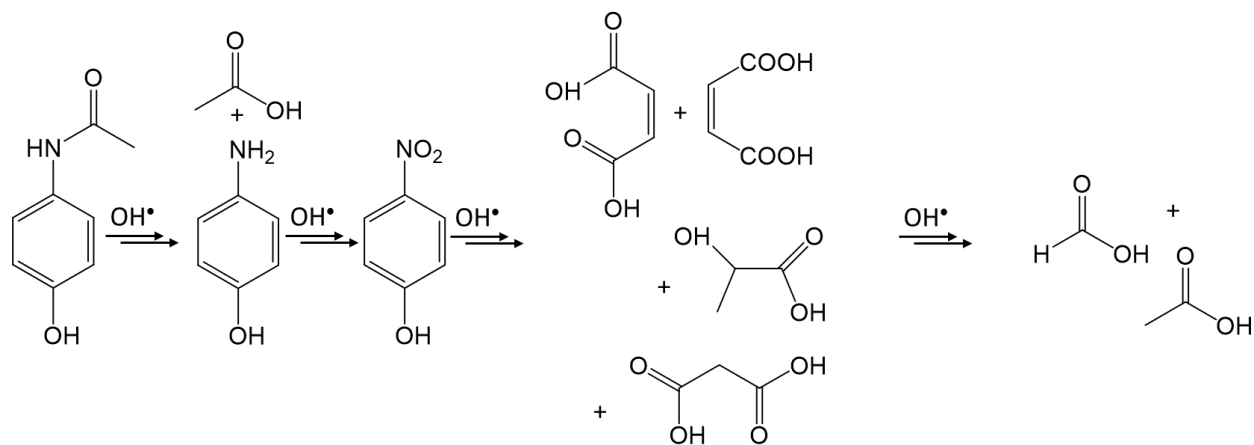


Figure S10. (a) Time dependent UV-Vis spectra of the battery catholyte in absence of Fe^{2+} ions. (b) NMR spectra of the catholyte before and after the battery discharge in absence of Fe^{2+} ions.



Scheme S3. Schematic representation showing the hydroxyl radical assisted degradation pathways of paracetamol forming formic acid and acetic acid. [Ref: 3]

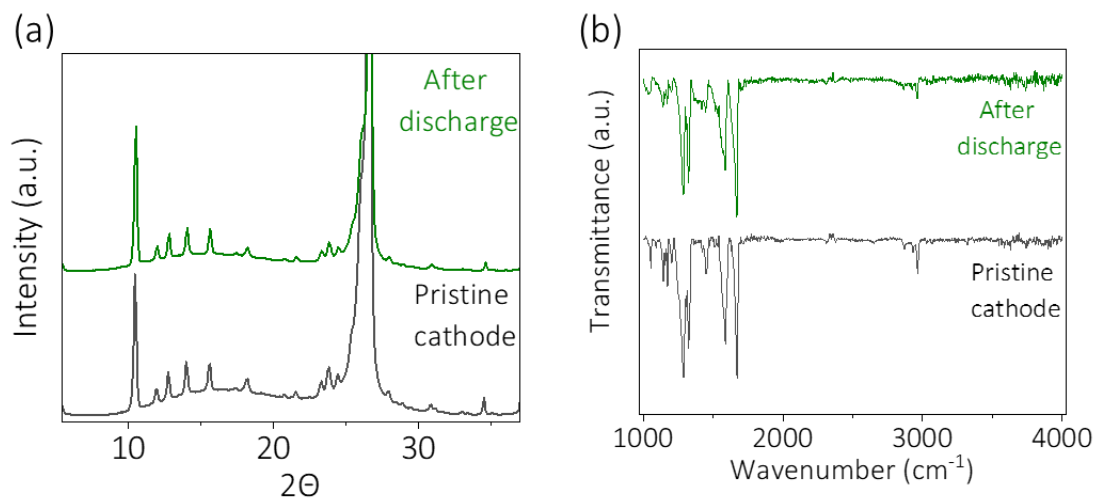


Figure S11. (a) XRD and (b) FTIR spectra of AQ/C composite electrode before and after battery discharge.

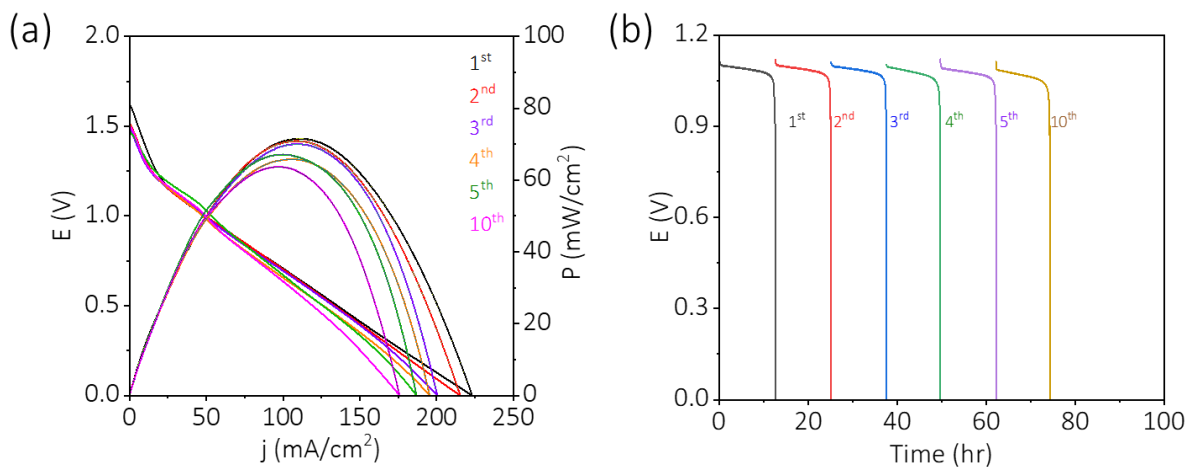
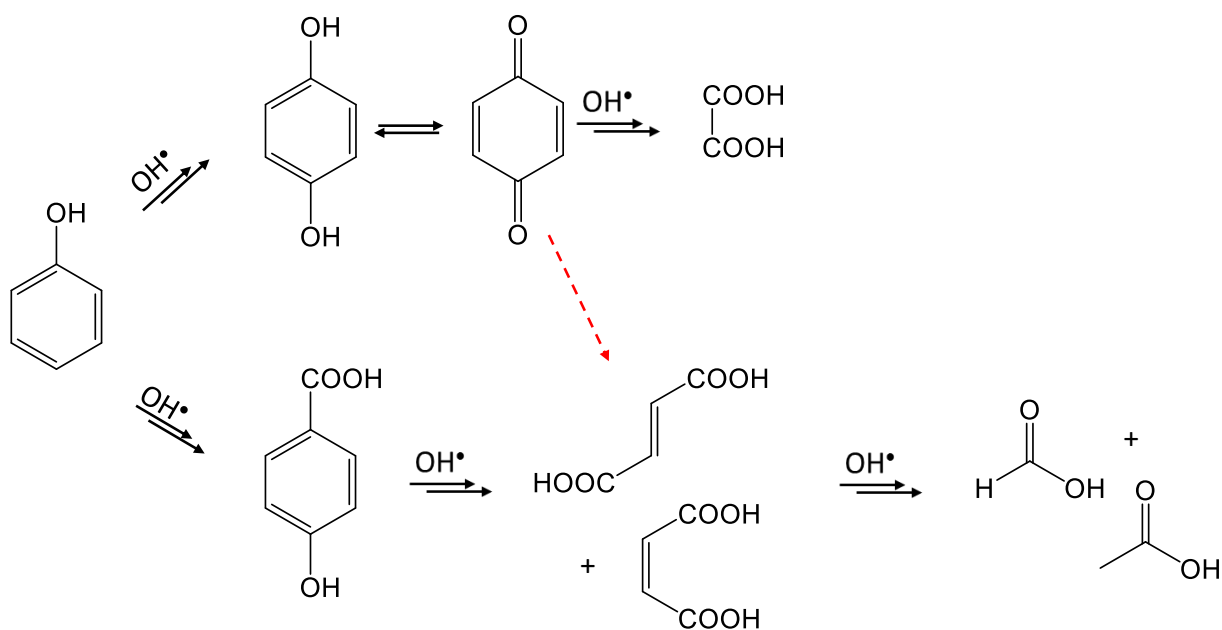


Figure S12. The performance of the pollutant degrading air battery for multiple cycles in O_2 -purged H_2SO_4 solution (pH 3) containing 0.2 mM Fe^{2+} and paracetamol (0.5 mM). (a) Polarization curves of the Zn-air battery and (b) the corresponding galvanostatic polarization at $10\text{ mA}/\text{cm}^2$.



Scheme S4. Schematic representation showing the hydroxyl radical assisted degradation pathways of phenol forming formic acid and acetic acid. [Ref: 4]

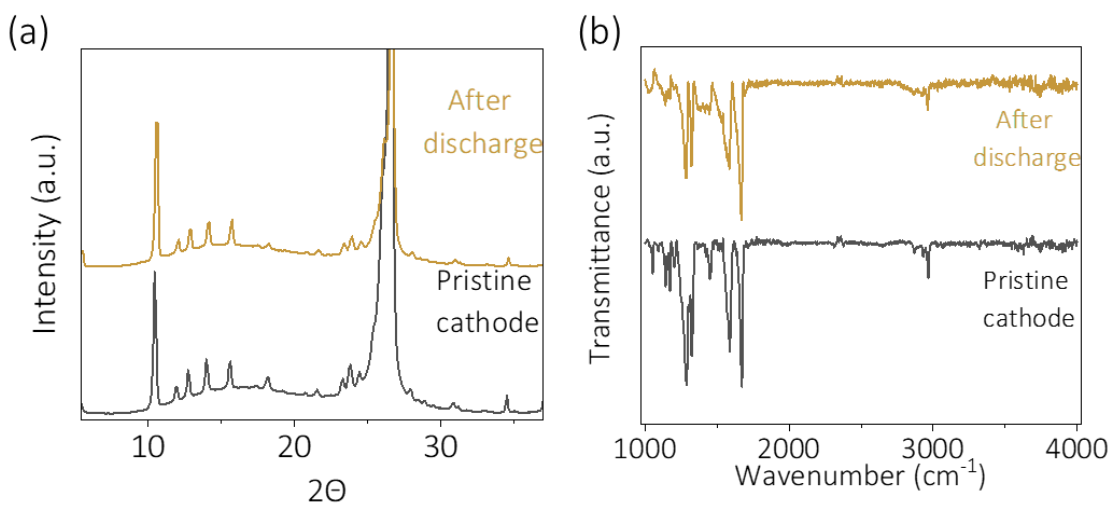


Figure S13. (a) XRD and (b) FTIR spectra of AQ/C electrode before and after battery discharge.

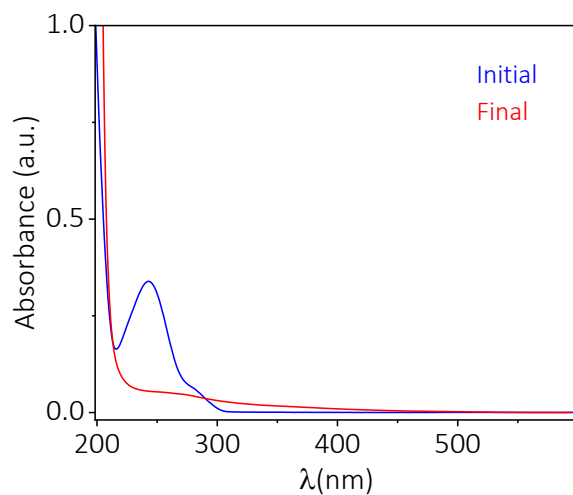


Figure S14. UV-Vis spectra of the electrolyte before and after discharge at 5 mA cm^{-2} .

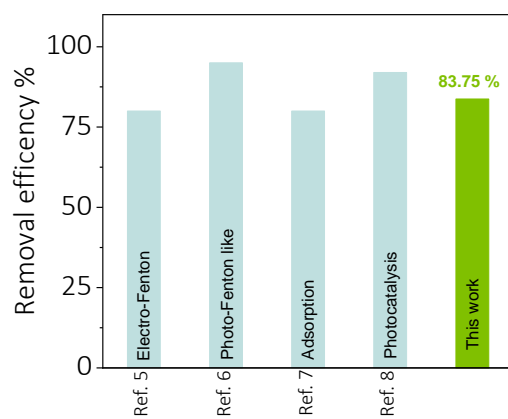


Figure S15. Degradation efficiency (%) demonstrated by various methods in comparison to this work.

References

1. J. M. Campos-Martin, G. Blanco-Brieva and J. L. G. Fierro, *Angew. Chemie Int. Ed.*, 2006, **45**, 6962–6984.
2. H. B. Vibbert, C. Bendel, J. R. Norton and A. J. Moment, *ACS Sustain. Chem. Eng.*, 2022, **10**, 11106–11116.
3. N. Villota, J. M. Lomas and L. M. Camarero, *J. Photochem. Photobiol. A Chem.*, 2016, **329**, 113–119.
4. G. Yang, H. Chen, H. Qin, X. Zhang and Y. Feng, *Can. J. Chem. Eng.*, 2017, **95**, 1518–1525.
5. X. Zheng, M. Gao, C. Liang, S. Wang and X. Wang, *Electrochim. Acta*, 2022, **428**, 140910.
6. A. Abdelhaleem, H. N. Abdelhamid, M. G. Ibrahim and W. Chu, *J. Clean. Prod.*, 2022, **379**, 134571.
7. G. Sivarasan, V. Manikandan, S. Periyasamy, M. S. AlSalhi, S. Devanesan, P. S. Murphin Kumar, R. rao Pasupuleti, X. Liu and H.-M. Lo, *Environ. Res.*, 2023, **227**, 115723.
8. M. Chijioke-Okere, A. H. Abdullah, Z. A. Mohd Hir, J. I. Alinnor and E. E. Oguzie, *Inorg. Chem. Commun.*, 2023, **148**, 110377.